Applied Catalysis B: Environmental 180 (2016) 758–765

Contents lists available at ScienceDirect

Applied Catalysis B: Environmental

journal homepage: www.elsevier.com/locate/apcatb

Carbon supported Pd-based bimetallic and trimetallic catalyst for formic acid electrochemical oxidation

Shuozhen Hu[a], Fabian Munoz[b], Jennifer Noborikawa[b], John Haan[b], Louis Scudiero[c,*], Su Ha[a,**]

[a] The Gene and Linda Voiland School of Chemical Engineering and Bioengineering, Washington State University, Pullman, WA 99164, United States
[b] Department of Chemistry and Biochemistry, California State University, Fullerton, CA 92831,United States
[c] Chemistry Department and Materials Science and Engineering Program, Washington State University, Pullman, WA 99164, United States

ARTICLE INFO

Article history:
Received 20 March 2015
Received in revised form 18 June 2015
Accepted 14 July 2015
Available online 18 July 2015

Keywords:
Pd-based bimetallic and trimetallic alloys
XPS
d-Band center
XRD
Formic acid electrochemical oxidation

ABSTRACT

The electronic structure and electrochemical performance of carbon supported Pd-based bi- and trimetallic nanoparticles are investigated. Pd/C, PdNi/C, PdCu/C, and PdNiCu/C alloys with face centered cubic crystal structure are synthesized by the one-step salt reduction method. The activities for these alloys toward the formic acid electrochemical oxidation measured by cyclic voltammetry (CV) display significant current density increase compared to that of Pd/C. An improvement in activity by a factor of 2 and 4 is measured when the data is normalized by electrochemical surface area (ECSA) and by Pd mass, respectively. A downward shift of the averaged d-band center relative to the Fermi level is observed for Pd-based alloys compared to Pd/C by X-ray photoelectron spectroscopy (XPS) measurements. The relationship between activity and the average d-band center displays a volcano shape for these alloys. Among the samples that we prepared for this study, PdNiCu/C alloy shows the best activity with the d-band center of 2.64 ± 0.10 eV. From CO stripping measurements the PdCu/C and PdNiCu/C alloys show less CO adsorption than Pd/C with PdCu/C showing the best stability toward the formic acid electrochemical oxidation.

1. Introduction

Low temperature proton exchange membrane fuel cells (PEMFCs) have generated great interest as potential power sources [1,2]. When hydrogen is used as the energy carrier, PEMFC has the best performance with a power density of 320 mW cm^{-2} at 20 °C and water is the only byproduct [3]. Since hydrogen gas has low energy density by volume, in order to compete with the high energy density of conventional logistic fuels, high-pressure or liquefied hydrogen needs to be used and stored in a compact container. However, safely storing high-pressure hydrogen is technologically and economically challenging [4]. To avoid the hydrogen storage problem, methanol has been recognized as the energy carrier and is directly fed to PEMFCs. Under this operating condition, even though methanol has high energy density (4900 Wh/L), the initial cell performance is significantly reduced due to slow methanol oxidation kinetics [5] and high methanol crossover through Nafion® membrane [6]. Owing to these disadvantages of using methanol or hydrogen, formic acid attracts researchers' attention as an alternative fuel and has been tested as the novel energy carrier for PEMFCs since 2002 [7]. Like methanol, formic acid is liquid under ambient conditions and easy to store and transport. However, unlike methanol, its electrochemical oxidation activity is unusually high [5]. Thus, direct formic acid fuel cells (DFAFCs) offer both fast anode kinetics (similar to hydrogen PEMFCs) and easy fuel storage (similar to DMFCs). Furthermore, formic acid exhibits low crossover through Nafion® membrane allowing high concentrations of formic acid (up to 15 M) to be used in the fuel cell without any critical performance drops [6,8,9]. Moreover, CO_2 can be electrochemically reduced to formic acid with high selectivity over metal electrodes (*e.g.*, In and Sn) in aqueous solutions at pH about 3 [10,11]. During the CO_2 electrochemical reduction, the electrical energy can be provided from hydro, wind, solar, tidal or nuclear energies [10]. Thus, by combining DFAFCs with the CO_2 electrochemical reduction process, the potential use of CO_2-derived fuels in so-called regenerative DFAFC system holds interesting prospects for future energy systems based on non-fossil energy sources.

Among the anode catalysts in DFAFCs, Palladium (Pd) and Platinum (Pt) are the two main catalysts for the formic acid electrochemical oxidation [12–14]. Over Pt-based catalysts, formic acid

* Corresponding author.
** Corresponding author.
E-mail addresses: scudiero@wsu.edu (L. Scudiero), suha@wsu.edu (S. Ha).

http://dx.doi.org/10.1016/j.apcatb.2015.07.023
0926-3373/

oxidizes through an indirect pathway, which involves the formation of CO as an intermediate species [7]:

$$Pt + HCOOH \rightarrow Pt-CO + H_2O \quad (1)$$

$$Pt + H_2O \rightarrow Pt-OH + H^+ + e^- \quad (2)$$

$$Pt-CO + Pt-OH \rightarrow 2Pt + CO_2 + H^+ + e^- \quad (3)$$

On the other hand, Pd-based catalysts oxidize formic acid *via* a direct pathway where the CO formation intermediate step is absent [15]:

$$Pd + HCOOH \rightarrow Pd-X \rightarrow Pd + 2H^+ + 2e^- \quad (4)$$

However, the formic acid electrochemical oxidation activity over carbon supported Pd catalysts is still low compared to that of hydrogen over carbon supported Pt catalysts [3]. Even though the Pd-based catalysts mainly oxidize the formic acid *via* the direct pathway, a small amount of formic acid is still oxidized *via* the indirect pathway [16,17]. Consequently, CO slowly accumulates over the Pd-based catalysts and leads to the poor long-term stability of the catalyst [18]. Additionally, Pd is a noble metal and very expensive. Hence, it is necessary to investigate less expensive Pd-based catalysts and improve its overall electrochemical performance.

It has been found that bimetallic and trimetallic catalysts show better performance than monometallic catalysts. For example, Liu et al. reported that the Pd_5Ru_1/C shows better electrocatalytic activity than the Pd/C for the formic acid oxidation due to the weakening of the adsorption strength of CO on Pd through the interaction between Pd and Ru [19]. Du et al. has also found that PdNi alloy nanowires are highly active catalysts for the electro-oxidation of formic acid [20]. PdAu supported on functionalized graphene nanoplatelets were studied by Maiyalagan et al. and displayed an increased activity for formic acid by a factor of 3 compared to that of Pd/Vulcan XC-72 [21]. Jiang et al. have successfully synthesized Ag@Pd core@shell nanotubes and obtained better CO tolerance and activity than that of Pd black with the same Pd loading [22]. Wang et al. synthesized Pd_4Co_2Ir/C and obtained higher current density and much better stability than Pd/C [23]. PdNiAg/C trimetallic nanoparticles were also investigated by Yurderi et al. as the catalyst for dehydrogenation of formic acid and provided the lowest activation energy [24]. All these studies have indicated that Pd-based bi- and trimetallic catalysts show an improved electrochemical activity and stability toward formic acid oxidation compared to pure Pd. Studies also show that the electronic property of Pd is altered by adding transition metals [25–27]. However, there is a lack of fundamental understanding on how these added transition metals interact with Pd to influence its electronic property and affect the overall formic acid electrochemical oxidation performance. Understanding such fundamental relationship can significantly help us to efficiently find better Pd-based catalysts for the formic acid electrochemical oxidation. Furthermore, the cost of the Pd-based catalysts can be reduced because less amount of Pd would be used in the catalyst synthesis when it alloys with other inexpensive transition metals. Thus, Pd-based bimetallic and trimetallic catalysts displaying improved formic acid oxidation activity and stability at a lower cost can be of high interest in the development of high performance DFAFCs.

The objective of this study is to investigate the relationship between the electronic structure and the electrochemical activity toward the formic acid oxidation reaction of the synthesized Pd-based bimetallic (PdCu/C and PdNi/C) and trimetallic (PdNiCu/C) alloys. These nanoparticle alloys were synthesized *via* a one-step metal salt reduction method. The particle size and dispersion of the supported Pd-based catalysts were obtained by transmission electron microscopy (TEM). X-ray diffraction (XRD) measurements confirmed the alloy formation. The electronic structure in terms of valence band and d-band centers of these catalysts was studied by X-ray photoelectron spectroscopy (XPS). The activity and stability of these Pd-based alloys toward the formic acid electrochemical oxidation were measured by cyclic voltammetry (CV) and chronoamperometry (CA).

2. Experimental

2.1. Pd-based alloys synthesis

Pd-based alloys were synthesized by the metal salt reduction method with the total metal loading of about 40 wt.% [28]. Activated carbon (Vulcan XC-72) was first treated by stirring it in 10 M hydrochloric acid for 12 h and then rinsed with Millipore® water until the pH reached 7. 100 mg of the treated activated carbon was dispersed in ca. 15 mL Millipore® water under ultra-sonication. Palladium chloride (H_2PdCl_4, Aldrich) and copper chloride ($CuCl_2$, Aldrich) solutions were mixed with the nominal atomic ratio of Pd:Cu = 3:1 and dissolved into 800 mL Millipore® water. 1 mL of 5 g/L polyvinyl alcohol (PVA) was added to the solution as the capping agent. Then, the 100 mg dispersed activated carbon was added to the precursor solution under sonication to form a slurry. 50 mL of 5 g/L reducing agent, sodium hypophosphite (NaH_2PO_2, Aldrich) was added drop-wise (ca. total 40 min) to synthesize the nanoparticles. Finally, 10 M sodium hydroxide (NaOH) was added to adjust the pH to 11. The carbon supported nanoparticle solution was stirred for 1 h under ambient conditions. After settling, the mixture solution was filtered and dried overnight. PdNi/C alloy was synthesized using the same method with nickel chloride ($NiCl_2$, Aldrich) as the precursor. PdNiCu/C alloy was prepared from the same precursor with the atomic ratio of Pd:Ni:Cu = 2:1:1. As a reference, Pd/C was also synthesized using the same method. To further clean the catalysts and strength the alloy formation, all the Pd-based alloys and Pd/C were annealed in Ar at 400 °C for 30 min. The phase diagram of bulk PdCu [29] and PdNi [30] systems show that both PdCu and PdNi alloys with 75 at.% Pd form a fcc crystal structure and are independent of the annealing temperature. Thus, the annealing process is not expected to affect the crystallinity of the Pd-based alloys.

2.2. Physical characterization

Images of the Pd-based bi- and trimetallic catalysts were obtained by TEM (Philips CM-200) and the particle size was estimated by using the ImageJ software. The crystal structure of these alloys was confirmed by X-ray diffraction (XRD) using the Rigaku Miniflex-600. The 2θ range of 35–80° with 0.01° intervals was used with the Cu Kα radiation source ($\lambda = 1.5406$ Å) operated at 40 kV–15 mA at room temperature.

2.3. Electrochemical analysis

The electrochemical measurements were performed on a Solartron Sl1287 Electrochemical Interface at a scan rate of 20 mV/s. A three-electrode system was used with a Pt mesh as counter electrode and an Ag/AgCl (3 M KCl) electrode as reference electrode. The glassy carbon electrode coated with the Pd-based alloy catalysts was used as working electrode. Before each measurement, high purity N_2 gas was bubbled through the electrolyte for 30 min to remove oxygen. The electrochemical active surface areas (ECSA) of the Pd-based bi- and trimetallic catalysts were calculated based on the charge of the Pd-oxide stripping peak [31] and used to normalize the current densities. All the electrochemical data shown here are referred to reversible hydrogen electrode (RHE).

Catalyst inks were prepared to attach the samples to the glassy carbon electrode. First, certain amount of each catalyst was dis-

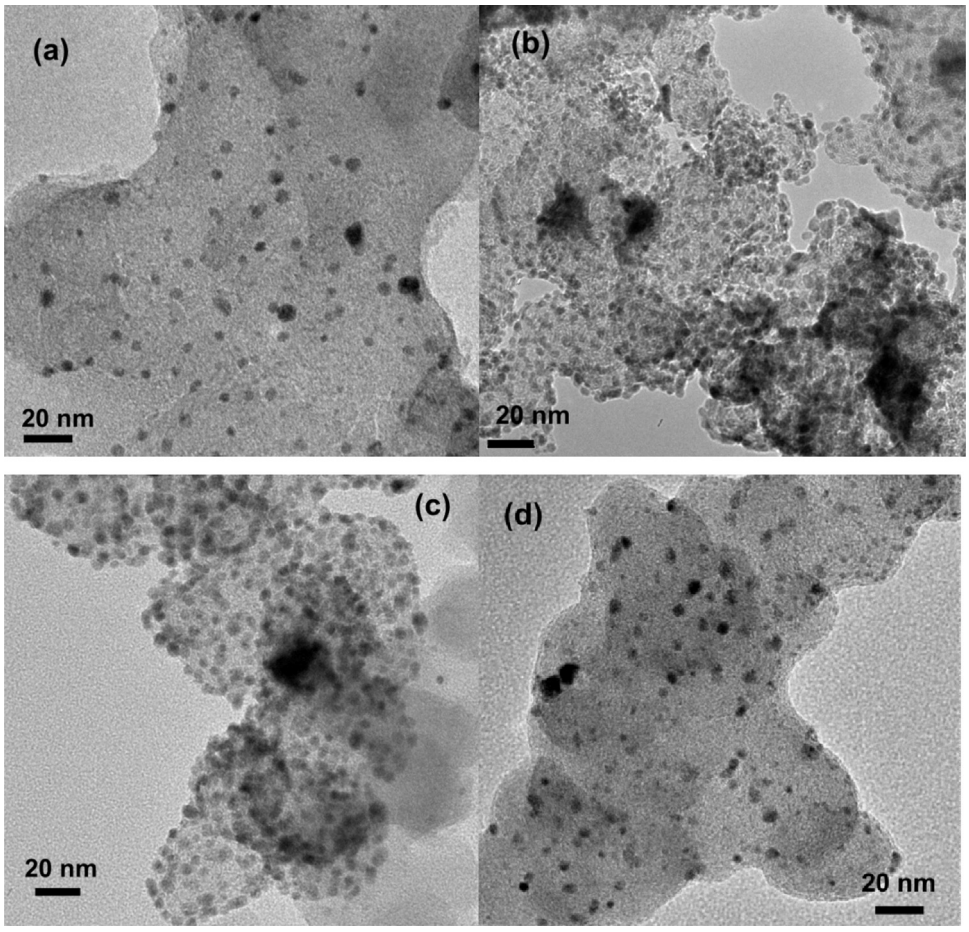

Fig. 1. TEM images of Pd/C (a), PdCu/C (b), PdNi/C (c), and PdNiCu/C (d).

persed in Millipore® water to prepare 5 mg/mL suspension. Then, 5 wt.% Nafion® solution (Dupont) was added to give a 20 wt.% Nafion® in the catalyst layer when dried. Finally, the total amount of 50 μL of each ink was dropped over the glassy carbon electrode and dried under a heating lamp.

CO stripping voltammetry was performed by running chronoamperometry in 0.5 M H_2SO_4 with bubbling CO gas for 1 h at 0 V *vs.* RHE. Following this, N_2 gas was bubbled to remove the CO in the solution. Then, cyclic voltammetry (CV) was run at 20 mV/s. Only the CO stripping part of the CV is shown.

2.4. X-ray photoelectron spectroscopy analysis

X-ray photoelectron spectroscopy (XPS) was performed on a Kratos AXIS-165 with a monochromatized Al Kα X-ray anode (1486.6 eV). The spectrometer was calibrated against both the Au $4f_{7/2}$ peak at 84.0 eV and the Ag $3d_{5/2}$ peak at 368.3 eV. For the XPS measurements, the samples were further cleaned by Ar^+ sputtering to remove the remaining precursor compound. The ion gun parameters used was 15 mA @ 4 kV and sputter time of 6 min. The valence bands were analyzed using commercial CasaXPS software and all spectra were smoothed using the Savitzky–Golay algorithm with a kernel of 5 points.

3. Results and discussion

3.1. Physical characterization

Fig. 1 shows TEM images of the Pd/C, PdCu/C, PdNi/C and PdNiCu/C nanoparticles dispersed on activated carbon. The average particle size for these alloys calculated with the ImageJ software is listed in Table 1. The particle size ranges from 4.3 ± 0.4 nm for PdCu/C to 5.8 ± 0.2 nm for PdNi/C. The atomic ratio of PdNi/C, PdCu/C and PdNiCu/C catalysts obtained by XPS is also summarized in Table 1. Since the general detection depth of XPS measurements is around 10 nm, which is larger than the particle size of all the alloys synthesized in this work, the composition detected by XPS indicates both surface and bulk atomic percentage of the Pd-based alloys.

Table 1
Particle size and composition for the supported Pd-based bimetallic and trimetallic catalysts.

Sample	Size (nm)	Composition by XPS (atomic %)
PdNiCu/C	4.9 ± 0.5	$Pd_{57}Ni_{13}Cu_{30}$
PdCu/C	4.3 ± 0.4	$Pd_{59}Cu_{41}$
PdNi/C	5.8 ± 0.2	$Pd_{81}Ni_{19}$
Pd/C	4.9 ± 0.5	Pd_{100}

3.2. X-ray diffraction analysis

The XRD patterns of the Pd-based alloys and Pd/C are shown in Fig. 2. All the samples show Pd(1 1 1), Pd(2 0 0) and Pd(2 2 0) peak at around 40.3°, 46.6° and 68.0°, respectively, indicating that the synthesized Pd/C and the Pd-based alloys have a face centered cubic (fcc) crystal structure [19,32,33]. Fig. 2b exhibits the XRD result in the narrow range between 35° and 45° where the Pd(1 1 1) peak is well resolved. In this range the peak of (1 1 1) plane for all Pd-based alloys shifts to higher 2θ value compared to that of Pd/C. This shift indicates that the transition metal atoms M (M = Cu, Ni

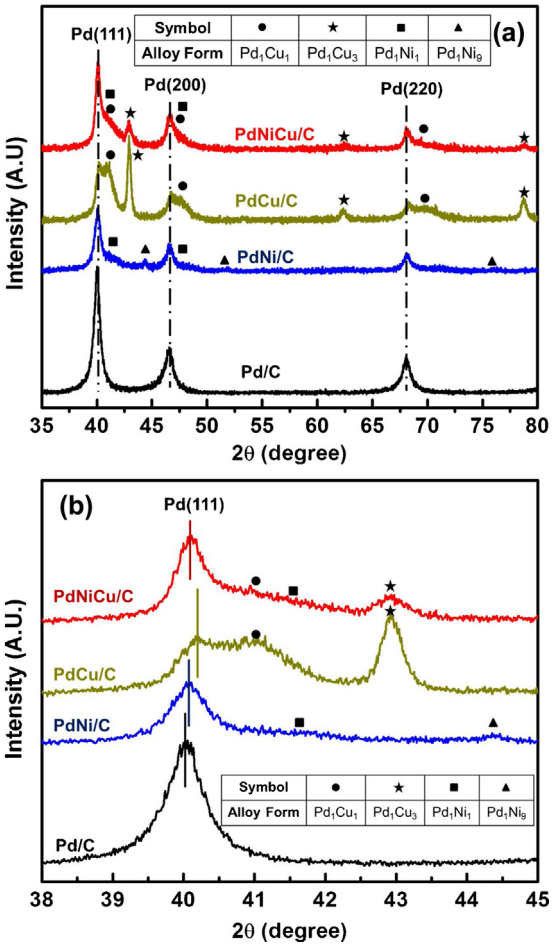

Fig. 2. Full range XRD (a) and blow up of the XRD in the range of 38–45 degree (b) for Pd/C (black), PdNi/C (blue), PdCu/C (yellow), and PdNiCu/C (red). (For interpretation of the references to colour in this figure legend, the reader is referred to the web version of this article.)

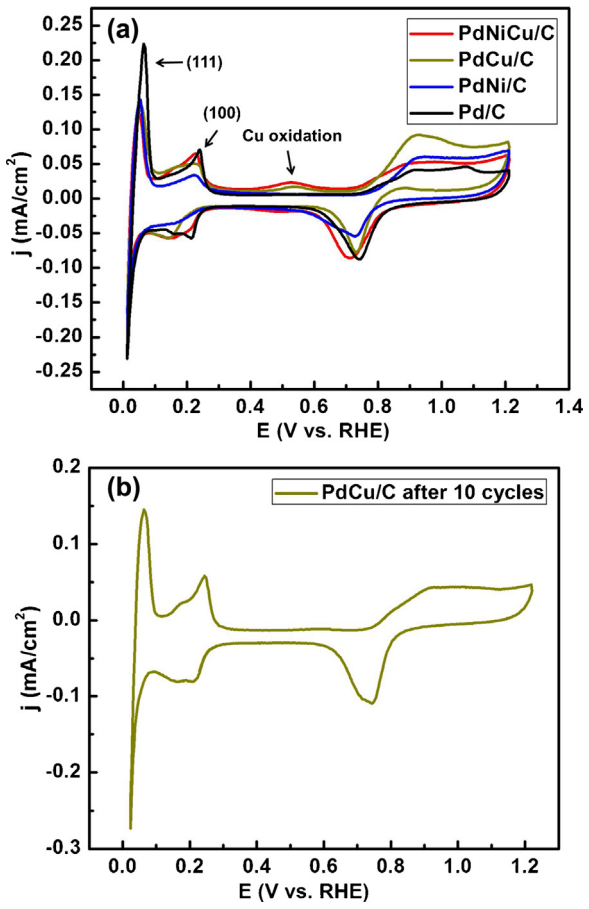

Fig. 3. (a) Cyclic voltammetry of Pd-based bi- and trimetallic catalysts in 0.5 M H_2SO_4 at a scan rate of 20 mV/s. (b) Cyclic voltammetry of PdCu–C after ten cycles in 0.5 M H_2SO_4 at a scan rate of 20 mV/s.

and mixed CuNi) are embedded into the Pd lattice to form Pd–M alloys. Among these alloys, PdCu/C displays the largest shift, which indicates that more Cu atoms are present into the Pd lattice than NiCu and Ni atoms in PdNiCu/C and PdNi/C alloys, respectively. This result is consistent with the composition of these alloys measured in atomic % by XPS (see Table 1). Additionally, two extra peaks at 41.2° and 43.1° are observed for the PdCu/C and PdNiCu catalysts. These peaks can be assigned to Pd_1Cu_1 and Pd_1Cu_3 alloys, respectively [29,34,35]. Such results indicate that a region of the bulk PdCu/C and PdNiCu alloys have Pd:Cu with 1:1 atomic ratio (Pd_1Cu_1), and other bulk regions a 1:3 atomic ratio (Pd_1Cu_3). Similarly, the data for PdNi/C displays weak peaks around 41.5° and 44.3° due to only 19% loading of Ni. These features are assigned to Pd_1Ni_1 and Pd_1Ni_9 alloys, respectively [33]. The PdNiCu/C trimetallic catalyst displays peaks that are a combination of PdCu/C and PdNi/C compounds with distinct (Pd:Cu 1:3 ratio) and faint (Pd:Cu 1:1 and Pd:Ni 1:1 ratios) peaks. Because of the Ni loading in this sample is even lower than that in PdNi/C (only 13 at.%), the Pd_1Ni_9 is most likely lost in the noise and therefore not clearly detected. Thus, based on the XRD patterns obtained for all the samples, the synthesized Pd-based bi- and trimetallic catalysts are heterogeneous alloys with regions of different bulk atomic ratios.

3.3. Electrochemical characterization analysis

The cyclic voltammetry (CV) of Pd-based alloys and Pd/C in 0.5 M H_2SO_4 are shown in Fig. 3a. The anodic peak observed at around 0 V and 0.2 V (RHE) are for the hydrogen desorption from Pd(1 1 1) and Pd(1 0 0) planes [36]. The similarity in CV confirms that all the Pd-based alloys and Pd/C have the same crystalline structure. A peak observed at about 0.5 V (RHE) for the PdCu/C and PdNiCu/C alloys is due to the oxidation of exposed Cu ($Cu \leftrightarrow Cu^{2+} + 2e^-$, 0.34 V *vs.* RHE). Ni oxidation peak is not detected for the PdNi/C and PdNiCu/C alloy samples because the standard electrode potential of Ni ($Ni \leftrightarrow NI^{2+} + 2e^-$ is −0.275 V (RHE)) is much lower than the potential range we used in the CV measurements. The anodic peak observed at around 0.9 V (RHE) indicates that Pd-oxide is formed on the surface. Fig. 3b shows the CV data for the PdCu/C alloy after 10 cycles in 0.5 M H_2SO_4. The absence of Cu oxidation peaks indicates that all the exposed Cu atoms were removed during the CV cycles. In the case of Ni since the standard potential of Ni is lower than 0 V (RHE), any exposed Ni and NiO that could formed on the surface after exposure to ambient conditions will spontaneously dissolve in the 0.5 M H_2SO_4 [37]. In this study, all the electrochemical results shown are after 10 cycles in 0.5 M H_2SO_4 to remove exposed Cu, Ni and NiO, and only leave Pd on the surface.

3.4. Electrochemical oxidation of formic acid and electronic analysis of Pd-based alloys

Initial activities for the Pd/C and Pd-based alloys toward the formic acid electrochemical oxidation are measured by cyclic voltammetry tests in 0.5 M H_2SO_4 with 0.5 M formic acid (Fig. 4a). The maximum anodic current density for the formic acid oxidation is measured at about 0.5 V (RHE) for all samples. In general, the Pd-based alloys show better initial activity for the formic acid elec-

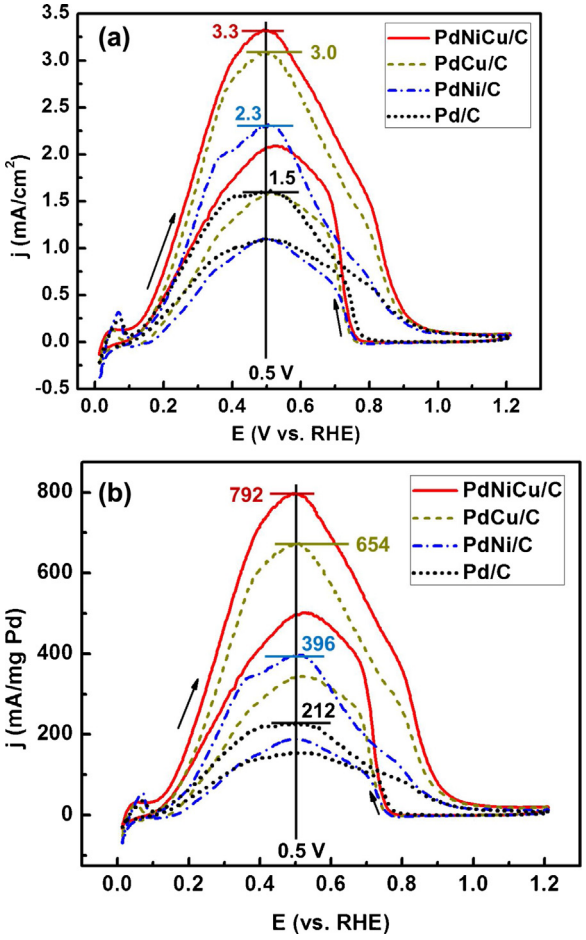

Fig. 4. Cyclic voltammetry of Pd-based bi- and trimetallic catalysts in 0.5 M H_2SO_4 with 0.5 M formic acid at a scan rate of 20 mV/s normalized by ECSA (a) and mass of Pd (b).

trochemical oxidation than the Pd/C. Among them, the PdNiCu/C trimetallic catalyst presents the best activity with a current density of 3.3 mA/cm^2. This represents an increase of 2.2 times more than the value obtained for the Pd/C. The bimetallic materials, PdNi/C and PdCu/C, also show an increase in activity by a factor of 1.5 and 2 compared to that of the Pd/C, respectively. The formic acid electrochemical oxidation reaction occurs over the Pd surface layer for each sample. As shown in their XRD data, the bulk phases of synthesized Pd-based bi- and trimetallic catalysts were heterogeneous alloys with regions of different bulk atomic ratios. Depends on the bulk composition of samples, their Pd surface layer would possess different activity toward the formic acid electrochemical oxidation reaction. For example, studies by Xu et al. and Ding et al. demonstrated that Pd-based alloys with different atomic ratio show different activity toward the formic acid oxidation [32,38]. For instance, Xu's study found that $Pd_{50}Cu_{50}$ has the best activity and stability toward the formic acid oxidation [32]. Furthermore, our previous results on the layered Pd–M films (M = Co, Cu, Ag, and Au) show that the activity of Pd surface toward the formic acid oxidation significantly changes depending on what bulk compositions were used to deposit the Pd film [39]. Since the bulk phases of the synthesized Pd-based bi- and trimetallic catalysts are heterogeneous alloys, the overall activity of their Pd surfaces toward the formic acid electrochemical oxidation would be a result of various contributions made by the different bulk alloy phases presented in each sample.

Fig. 4b displays the activity of the catalysts based on the mass of Pd. PdNiCu/C shows the most improvement with a factor of 3.7

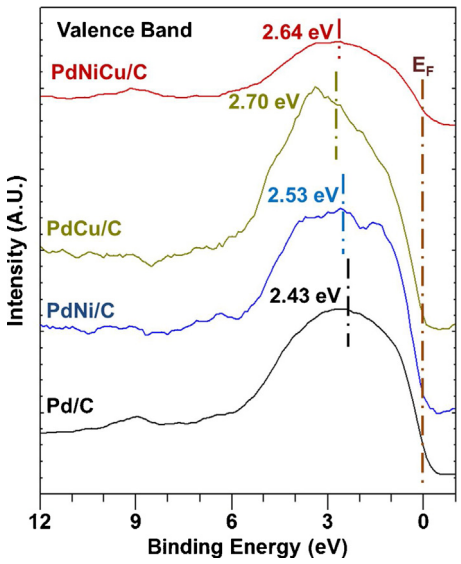

Fig. 5. XPS Valence band and d-band center for the Pd-based bi- and trimetallic catalysts.

(792 mA/mg Pd) activity enhancement when compared with the Pd/C (212 mA/mg Pd), followed by the PdCu/C (645 mA/mg Pd) and the PdNi/C (396 mA/mg Pd) alloys. The trimetallic catalyst exhibits the highest current density per mg of Pd. According to the atomic composition measured by XPS (shown in Table 1), there are 57% Pd and 43% NiCu mixture in PdNiCu/C alloy, and 59% Pd and 41% Cu in PdCu/C alloy. PdNiCu/C and PdCu/C alloys contain very similar amounts of Pd. With the similar amount of Pd, PdNiCu/C shows better electrochemical activity toward the formic acid oxidation than PdCu/C. Such result indicates that the NiCu mixture in PdNiCu/C alloy plays an important role in the activity enhancement. Since Cu and Ni do not catalyze the formic acid electrochemical oxidation, the NiCu must be altering the Pd in such a way that the oxidation rate is increased. In other words, Ni and Cu are improving the Pd activity toward the formic acid electrochemical oxidation. Detailed analysis of the NiCu mixture effect in the PdNiCu alloy is still under investigation. Nevertheless, the trimetallic catalyst shows the best Pd utilization for our study.

One possible effect is an electronic perturbation of the Pd surface [39]. To investigate the possible electronic effect generated by the addition of Ni and Cu to Pd on the activity toward the formic acid electrochemical oxidation, XPS valence bands of these samples were collected and are shown in Fig. 5. The d-band centers were calculated by integrating the normalized first moment of the density of state (DOS) that was approximated by the measured N(E) [40]. Since the general detection depth of XPS measurements is around 10 nm, which is larger than the particle size of all the alloy samples synthesized in this work, the estimated d-band center shown in Fig. 5 represents the average d-band center of each sample combining the contributions from both its Pd surface and heterogeneous bulk alloys. The bigger contribution would come from the bulk alloy because each sample contains more bulk atoms than the surface atoms. As discussed in the previous section, the surface of each sample should be consisted of pure Pd layer following their dealloying process in the CV cycles. Thus, the d-band center of each sample estimated from our valence XPS data would not represent the true d-band center of its corresponding Pd surface layer where the reaction occurs [41]. However, it is important to point out that the Pd surface layer would be directly interfacing with the bulk alloy for each sample. As the d-band center of bulk alloys are changing in one direction, the Pd surface layers that are interfacing with those alloys should also change in the same direction. Based on this argu-

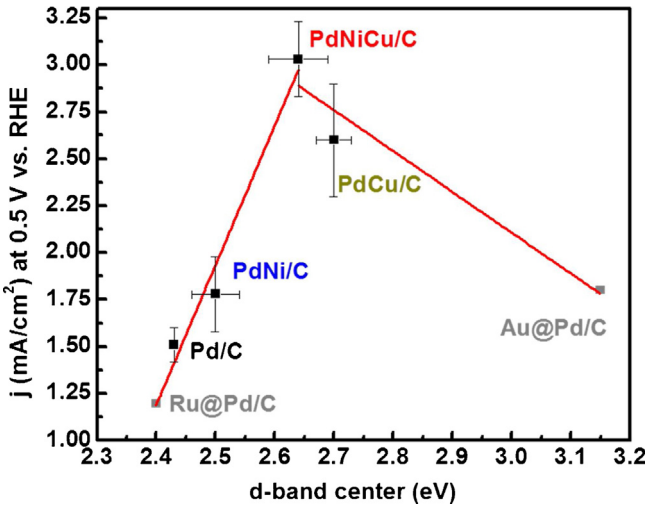

Fig. 6. Relationship between the d-band center and the current at 0.5 V *vs.* RHE for the Pd-based bi- and trimetallic catalysts. The Ru@Pd/C and Au@Pd/C results from our previous study are incorporated and shown in gray color.

ment, our average d-band centers shown in Fig. 5 can be used to investigate how the electronic structure of Pd surface layer would be affected by introducing different bulk alloy phases.

As shown in Fig. 5, the d-band center of the PdNi/C is 2.53 eV and of the PdCu/C is 2.70 eV. They both shift away from the Fermi level compared to Pd/C (2.43 eV). It is known that the particle size affects the d-band center [42]. However, since the particle sizes in this study are about 5 nm, its effects on the d-band center shifts should be negligible. Thus, the d-band center shifts are a result from the charge transfer from Pd to the 3d transition metals Ni and/or Cu. The d-band center position can be significantly affected by (1) the fraction of empty state difference between these dissimilar metals [43–45], and (2) the valence band structures of Cu and Ni. For instance, Cu has a half empty 4s band that can act as an electron donor or acceptor depending on the valence band of the dissimilar metal. However, Pd has a fully filled 4d band. Therefore, electrons will flow from the Pd 4d band into the 4s band of Cu as confirmed by our XPS valence band data (*i.e.*, decreased shoulder in the range of 0–2 eV). Similarly, Ni has an unfilled 3d band (d^8) and electrons would also flow from the Pd 4d to the Ni 3d. For the PdNiCu/C trimetallic catalyst, the detailed charge transfer between three elements is still under investigation. Nevertheless, the d-band center of PdNiCu/C is 2.64 eV, also shifted away from the Fermi level compared to that of the Pd/C and is located between PdNi/C and PdCu/C.

A relationship between the position of the d-band center and the formic acid oxidation current density measured at 0.5 V (RHE) for the Pd/C and Pd-based alloys reveals a volcano shape relationship (Fig. 6). Results from Ru@Pd/C and Au@Pd/C core@shell nanoparticles are incorporated in the plot in order to emphasize the volcano shape relationship. A detailed material characterization of these core@shell nanoparticles can be found in our previous publication [46]. As the d-band center for the catalysts investigated in this work shifts away from the Fermi level, the catalytic activity of the nanoparticles toward the formic acid electrochemical oxidation increases until reaching a maximum value at an optimum d-band center. Based on the samples that we investigated in this study, it seems that this optimum (or optimum range of) d-band center should be around 2.64 eV, which corresponds to the maximum current density of 3.3 mA/cm^2. The current density then decreases beyond this optimum value of the d-band center. This result agrees with our previous findings on the Pd-based bimetallic films [39,47]. Previous studies [48,49] also found that as the d-band center shifts away from the Fermi level (*i.e.*, the charge transfer from Pd to other transition metals), the bond strength between the adsorbate and Pd surface is weakened. This could also be the case for the formic acid electrochemical oxidation over Pd surface. We propose the following reaction mechanism to explain the volcano shape relationship shown in Fig. 6. During the formic acid electrochemical oxidation over the Pd surface, $HCOO_{ad}$ (HCOO–Pd) is first formed as a reactive intermediate species *via* breaking the O—H bond in HCOOH (Eq. (6)) [17,50,51]. Once $HCOO_{ad}$ is formed, it then can decompose to CO_2 through a transition state, for example a tilted bridge-bonded configuration [51,52] with two Pd—O bonds and a H atom approaching to the Pd site (Eq. (7)).

$$HCOOH + Pd \rightarrow HCOO - Pd + H^+ + e^- \quad (6)$$

$$HCOO - Pd \rightarrow Pd - H + CO_2 \quad (7)$$

$$Pd - H \rightarrow Pd + H^+ + e^- \quad (8)$$

By shifting the Pd d-band center away from the Fermi level, the bond strength between the intermediate species ($HCOO_{ad}$) and Pd becomes weaker, for example the two Pd—O bonds. Consequently, Pd—O bond scission requires less energy (*i.e.*, $HCOO_{ad}$ decomposition is easier) as in the case of the PdNi/C and PdNiCu/C samples. However, as the d-band center further shifts away from its optimum value (for the PdCu/C sample), the Pd—O bond becomes too weak resulting in the formation of less key intermediate species ($HCOO_{ad}$). Furthermore, the Pd—H bond (shown in Eq. (7)) would become too weak as well, which makes the decomposition of $HCOO_{ad}$ into CO_2 by breaking its C—H bond becomes more difficult too. The overall result is a decrease in activity. Thus, Pd-adsorbate bond strength can be optimized by shifting the d-band center to its optimum value (*i.e.*, 2.64 ± 0.10 eV for our study), and the catalysts shows the best activity toward the formic acid oxidation. At this point, we do not have *in-situ* FTIR data to support our proposed reaction mechanism for explaining the volcano shape relationship between activity and d-band center. Thus, it is only speculation at this point. We are, however, currently planning *in-situ* FTIR testing of bimetallic and trimetallic catalysts to provide direct evidence on how the bond strength of key intermediate species is changing as the average d-band center of each sample is modified.

Studies have shown that the electrochemical activity of Pd-based catalyst is also related to the particle size [53,54]. Within the size range of 2.7–9.0 nm, a classical volcano plot of catalytic activity *vs.* particle size was obtained and the optimal Pd particle size was 5–7 nm. In our study, most of the particles investigated are about 5 nm in diameter therefore the size effect should not be expected to play a major role. The formic acid electrochemical oxidation activity is also highly dependent on the catalyst surface structure, *i.e.*, bifunctional effect. For example, in PdAu alloys the promotional effect of Au and the absence of continuous Pd sites suppress the poisoning effect of CO [21]. However, in this study, all the Pd-based alloy catalysts were tested after removing the surface Cu, Ni or NiO by 10 cycles CV performed in 0.5 M H_2SO_4. Thus, only Pd is on the surface to electrochemically oxidize formic acid and the bifunctional effect is avoided.

3.5. Electrochemical stability of Pd-based alloys toward the formic acid oxidation

Normalized chronoamperometry (CA) results for the PdNiCu/C, PdCu/C and Pd/C are shown in Fig. 7. Fig. 7(a) is normalized by the ECSA, while Fig. 7(b) is normalized by the mass of Pd. Both PdNiCu/C and PdCu/C alloys show a better stability than that of Pd/C within one hour. It has been suggested that the CO_{ad} accumulates slowly on Pd surface during the formic acid electrochemical oxidation either from the indirect pathway [17,51] or reduction of CO_2

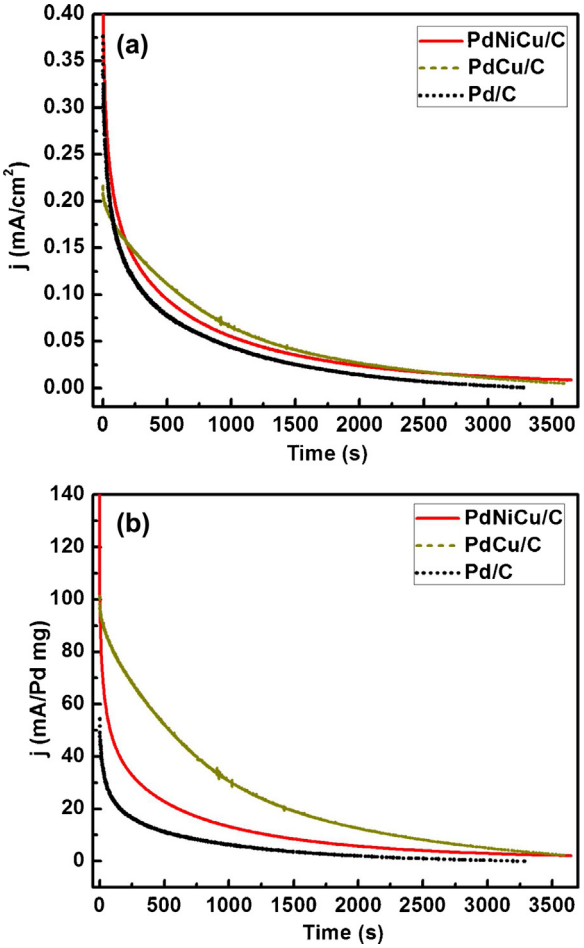

Fig. 7. Chronoamperometry of Pd–C, PdCu–C, and PdNiCu–C catalysts in 0.5 M H_2SO_4 with 0.5 M formic acid at a fixed potential of 0.16 V *vs.* RHE normalized by ECSA (a) and mass of Pd (b).

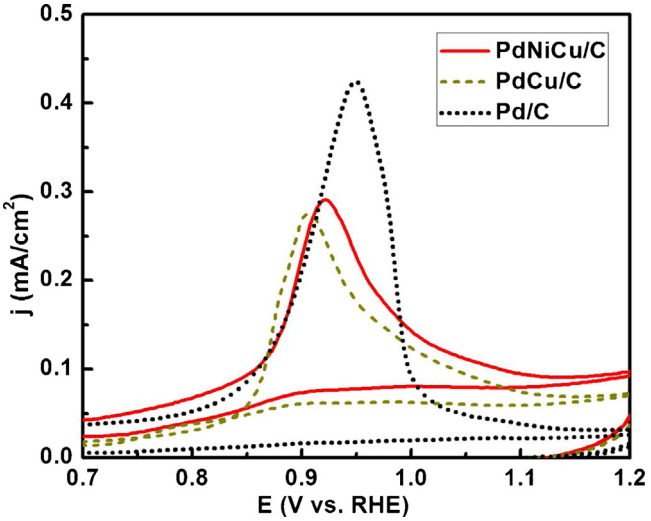

Fig. 8. CO stripping for the Pd-based bi- and trimetallic catalysts.

[16,55]. Consequently, Pd loses activity, as shown in Fig. 7. To support this hypothesis and explain the stability improvements of the bi- and trimetallic catalysts, the CO stripping test was performed (see Fig. 8). The CO stripping peak potentials for the PdNiCu/C and PdCu/C alloys were measured at 0.922 V and 0.907 V (RHE), respectively. Both CO stripping peak potential values are lower than the

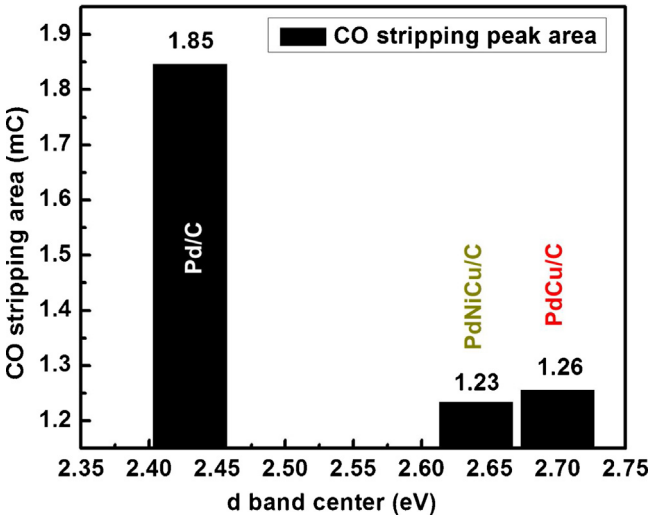

Fig. 9. Relationship between the d-band center and CO stripping area for the Pd-based bi- and trimetallic catalysts.

value of 0.950 V measured for the Pd/C sample. The lower potential indicates that the Pd—CO bond becomes weaker on the alloyed samples. Upon alloying of Pd with Ni or Cu the d-band center of Pd shifts away from the Fermi level resulting in less electron back-donation from the Pd surface to CO [56–58]. In addition, the areas under the CO stripping peaks for Pd/C, PdCu/C, PdNi/C and PdNiCu/C samples are estimated based on Fig. 8 and shows in Fig. 9. According to this estimation, the CO stripping areas for the bi- and trimetallic samples are about 1.5 times less than that of the Pd/C sample. The CO stripping data indicates a weaker Pd—CO bond strength and a reduction of adsorbed CO amount on the PdNiCu/C and PdCu/C alloy surfaces than on the Pd/C surface. By minimizing the CO poisoning step the long-term stability of both the PdNiCu/C and PdCu/C samples are improved when compared to that of the Pd/C sample.

4. Conclusion

Pd/C, PdNi/C, PdCu/C, and PdNiCu/C alloys are successfully synthesized by one-step salt reduction method. All the nanoparticles are very well dispersed on carbon support with an average size of about 5 nm. XRD patterns indicate that the crystal structure of the synthesized Pd/C and Pd-based alloys is face centered cubic, and that the alloys are mixtures of Pd–M alloys with different atomic ratios. The initial activities measured by CV experiments indicate that the trimetallic PdNiCu/C alloys display the most significant current density increase when compared to Pd/C. According to the XPS results, as Pd alloys with Ni and Cu, the d-band center of Pd-based alloys shifts away from the Fermi level (2.7 eV for PdCu/C, 2.63 eV for PdNiCu/C, and 2.53 eV for PdNi/C) compare to Pd/C (2.43 eV). A volcano shape plot is obtained for the relationship between initial activity and the d-band center for these catalysts. As the d-band center shifts away from the Fermi level, the activity increases until it reaches an optimum value, 2.64 eV, then decreases. This could be attributed to a weakening of the Pd-adsorbate bond strength down to its optimum value, which favors higher electrochemical activity. With further d-band center shift, the bond becomes too weak and less $HCOO_{ad}$ is formed. Thus, the activity toward the formic acid electrochemical oxidation would be reduced. In addition, with the d-band center shifting away from the Fermi level for PdCu/C and PdNiCu/C, there will be less electron back-donation to CO, which weakens the Pd—CO bond. As a result, lower CO stripping peak potential and peak area are obtained. Consequently, PdCu/C and

PdNiCu/C are poisoned at a slower rate and show the best stability toward formic acid.

Acknowledgements

Funding was provided by the National Science Foundation under Agreement 38135136, DMR-9503304 and CHE-1048600, the Petroleum Research Fund (PRF# 53133-UNI5), and grant funds from California State University, Fullerton.

References

[1] J.H. Wee, Renew. Sustain. Energy Rev. 11 (2007) 1720–1738.
[2] Y. Wang, K.S. Chen, J. Mishler, S.C. Cho, X.C. Adroher, Appl. Energy 88 (2011) 981–1007.
[3] Y.M. Zhu, Z. Khan, R.I. Masel, J. Power Sources 139 (2005) 15–20.
[4] X.W. Yu, P.G. Pickup, J. Power Sources 182 (2008) 124–132.
[5] M. Weber, J.T. Wang, S. Wasmus, R.F. Savinell, J. Electrochem. Soc. 143 (1996) L158–L160.
[6] K.J. Jeong, C.A. Miesse, J.H. Choi, J. Lee, J. Han, S.P. Yoon, S.W. Nam, T.H. Lim, T.G. Lee, J. Power Sources 168 (2007) 119–125.
[7] C. Rice, S. Ha, R.I. Masel, P. Waszczuk, A. Wieckowski, T. Barnard, J. Power Sources 111 (2002) 83–89.
[8] Y.W. Rhee, S.Y. Ha, R.I. Masel, J. Power Sources 117 (2003) 35–38.
[9] X. Wang, J.M. Hu, I.M. Hsing, J. Electroanal. Chem. 562 (2004) 73–80.
[10] C. Oloman, H. Li, ChemSusChem 1 (2008) 385–391.
[11] S. Kapusta, N. Hackerman, J. Electrochem. Soc. 130 (1983) 607–613.
[12] S. Ha, R. Larssen, Y. Zhu, R.I. Masel, Fuel Cells 4 (2004) 337–343.
[13] Y.M. Zhu, S.Y. Ha, R.I. Masel, J. Power Sources 130 (2004) 8–14.
[14] S. Ha, R. Larsen, R.I. Masel, J. Power Sources 144 (2005) 28–34.
[15] R. Larsen, S. Ha, J. Zakzeski, R.I. Masel, J. Power Sources 157 (2006) 78–84.
[16] K. Jiang, H.X. Zhang, S.Z. Zou, W.B. Cai, Phys. Chem. Chem. Phys. 16 (2014) 20360–20376.
[17] H. Miyake, T. Okada, G. Samjeske, M. Osawa, Phys. Chem. Chem. Phys. 10 (2008) 3662–3669.
[18] J.L. Haan, K.M. Stafford, R.I. Masel, J. Phys. Chem. C 114 (2010) 11665–11672.
[19] Z.L. Liu, X.H. Zhang, S.W. Tay, J. Solid State Electrochem. 16 (2012) 545–550.
[20] C.Y. Du, M. Chen, W.G. Wang, G.P. Yin, ACS Appl. Mater. Interface 3 (2011) 105–109.
[21] T. Maiyalagan, X. Wang, A. Manthiram, RSC Adv. 4 (2014) 4028–4033.
[22] Y.Y. Jiang, Y.Z. Lu, D.X. Han, Q.X. Zhang, L. Niu, Nanotechnology 23 (2012).
[23] R.F. Wang, S.J. Liao, S. Ji, J. Power Sources 180 (2008) 205–208.
[24] M. Yurderi, A. Bulut, M. Zahmakiran, M. Kaya, Appl. Catal. B-Environ. 160 (2014) 514–524.
[25] N. Martensson, R. Nyholm, H. Calen, J. Hedman, B. Johansson, Phys. Rev. B 24 (1981) 1725–1738.
[26] R.E. Watson, J. Hudis, M.L. Perlman, Phys. Rev. B 4 (1971) 5.
[27] K.R. Harikumar, S. Ghosh, C.N.R. Rao, J. Phys. Chem. A 101 (1997) 536–540.
[28] J. Noborikawa, J. Lau, J. Ta, S. Hu, L. Scudiero, S. Derakhshan, S. Ha, J.L. Haan, Electrochim. Acta (2014).
[29] V. Mukundan, J. Yin, P. Joseph, J. Luo, S.Y. Shan, D.N. Zakharov, C.J. Zhong, O. Malis, Sci. Technol. Adv. Mater. 15 (2014).
[30] MTDATA, National Phys. Lab. (2015).
[31] P.N. Bartlett, B. Gollas, S. Guerin, J. Marwan, Phys. Chem. Chem. Phys. 4 (2002) 3835–3842.
[32] C.X. Xu, Y.Q. Liu, J.P. Wang, H.R. Geng, H.J. Qiu, J. Power Sources 199 (2012) 124–131.
[33] A. Dutta, J. Datta, J. Mater. Chem. A 2 (2014) 3237–3250.
[34] N.N. Kariuki, X.P. Wang, J.R. Mawdsley, M.S. Ferrandon, S.G. Niyogi, J.T. Vaughey, D.J. Myers, Chem. Mater. 22 (2010) 4144–4152.
[35] X.P. Wang, N. Kariuki, J.T. Vaughey, J. Goodpaster, R. Kumar, D.J. Myers, J. Electrochem. Soc. 155 (2008) B602–B609.
[36] N. Hoshi, K. Kida, M. Nakamura, M. Nakada, K. Osada, J. Phys. Chem. B 110 (2006) 12480–12484.
[37] E.A. Abdel-Aal, M.M. Rashad, Hydrometallurgy 74 (2004) 189–194.
[38] K.Q. Ding, L. Liu, Y.L. Cao, X.R. Yan, H.G. Wei, Z.H. Guo, Int. J. Hydrogen Energy 39 (2014) 7326–7337.
[39] S.Z. Hu, L. Scudiero, S. Ha, Electrochem. Commun. 38 (2014) 107–109.
[40] V.R. Stamenkovic, B.S. Mun, M. Arenz, K.J.J. Mayrhofer, C.A. Lucas, G.F. Wang, P.N. Ross, N.M. Markovic, Nat. Mater. 6 (2007) 241–247.
[41] J.-S. Kang, D.W. Hwang, C.G. Olson, S.J. Youn, K.-C. Kang, B.I. Min, Phys. Rev. B 56 (1997) 10605–10613.
[42] W.P. Zhou, A. Lewera, R. Larsen, R.I. Masel, P.S. Bagus, A. Wieckowski, J. Phys. Chem. B 110 (2006) 13393–13398.
[43] M. Arenz, V. Stamenkovic, T.J. Schmidt, K. Wandelt, P.N. Ross, N.M. Markovic, Phys. Chem. Chem. Phys. 5 (2003) 4242–4251.
[44] A. Ruban, B. Hammer, P. Stoltze, H.L. Skriver, J.K. Norskov, J. Mol. Catal. A-Chem. 115 (1997) 421–429.
[45] B.S. Mun, C. Lee, V. Stamenkovic, N.M. Markovic, P.N. Ross, Phys. Rev. B 71 (2005).
[46] S. Hu, S. Ha, L. Scudiero, ECS Trans. 64 (2014) 1121–1127.
[47] S.Z. Hu, L. Scudiero, S. Ha, Electrochim. Acta 83 (2012) 354–358.
[48] P.J. Berlowitz, D.W. Goodman, Langmuir 4 (1988) 1091–1095.
[49] J.R. Kitchin, J.K. Norskov, M.A. Barteau, J.G. Chen, J. Chem. Phys. 120 (2004) 10240–10246.
[50] E. Jeroro, J.M. Vohs, Catal. Lett. 130 (2009) 271–277.
[51] Y.Y. Wang, Y.Y. Qj, D.J. Zhang, C.B. Liu, J. Phys. Chem. C 118 (2014) 2067–2076.
[52] R.G. Sharpe, M. Bowker, J. Phys.-Condens. Matter 7 (1995) 6379–6392.
[53] Y. Suo, I.M. Hsing, Electrochim. Acta 55 (2009) 210–217.
[54] W.J. Zhou, J.Y. Lee, J. Phys. Chem. C 112 (2008) 3789–3793.
[55] M.H. Shao, J. Odell, M. Humbert, T.Y. Yu, Y.N. Xia, J. Phys. Chem. C 117 (2013) 4172–4180.
[56] B. Hammer, Y. Morikawa, J.K. Norskov, Phys. Rev. Lett. 76 (1996) 2141–2144.
[57] F. Gao, D.W. Goodman, Chem. Soc. Rev. 41 (2012) 8009–8020.
[58] P. Liu, J.K. Norskov, Phys. Chem. Chem. Phys. 3 (2001) 3814–3818.